IJE TRANSACTIONS B: Applications Vol. 35, No. 02, (February 2022) 471-480

International Journal of Engineering

Journal Homepage: www.ije.ir

Hybrid Massive MIMO Channel Model Based on Edge Detection of Interacting Objects and Cluster Concept

M. M. Tamaddondar*, N. Noori

Department of Communication Technologies ICT Research Center Institute, Tehran, Iran

P A P E R I N F O

Paper history:
Received 14 August 2020
Received in revised form 03 November 2021
Accepted 29 November 2021

Keywords:
Channel Model
Clustering
Edge Detection
Massive MIMO
Doppler Effect

A B S T R A C T

This paper presents a novel channel model based on the edge detection of the interacting objects (IOs) for massive multiple-input and multiple-output (MIMO) systems considering different propagation phenomena such as reflection, refraction, diffraction, and scattering occur at the edges of the IOs. This channel model also uses cluster concepts to model multipath components (MPCs). The time-variant condition of the channel as well as the Doppler effect is considered in this channel model. Also, the non-stationary property of the channel across the array axis can be observed in the simulations. Due to a large number of antenna elements utilized in the massive MIMO systems, the spherical wavefront is assumed instead of the plane wavefront which is used in the conventional MIMO channel model. The central limit theory is also utilized to model the MPCs of each cluster. Furthermore, specific channel characteristics such as channel impulse response (CIR), angle of arrival (AoA) as well as time of arrival (ToA) are extracted in the simulations of the channel.

doi: *10.5829/ije.2022.35.02b.23*

1. INTRODUCTION

In the fifth generation (5G) of wireless communication systems, significant improvement in energy and spectrum efficiency, as well as reliability, is considered in compare to the previuos generation [1]. Millimeter wave technology is an innovation that allows benefiting from large bandwidths and very high data rates. However, this technology imposes the constraints of high attenuation and blockage to the system design. To achieve projected theoretically specifications, massive MIMO is regarded as a cornerstone and the most promising technology for meeting 5G wireless communication systems [2]. A large number of antenna elements in massive MIMO systems yield to increase the channel capacity, spatial resolution, energy, and spectral efficiency as well as linkage reliability [3, 4]. Massive MIMO systems also provide superior channel orthogonality and more channel stability than conventional MIMO systems [5]. Another essential objective behind the use of massive MIMO in 5G is to scan the overall pattern of the antenna for interference reduction and long distance communication [2]. Three dimensional (3D) channel modeling has an important role in accurate designing and a better understanding of the wireless communication systems [4, 6]. Also, massive MIMO benefits severely depend on accurate channel estimation. The parametric channel model is a way to regularize the channel estimation, which exploits the fact that a signal arrives at the receiver via a limited number of MPCs [7, 8]. The channel model should consider several emerging features of massive MIMO such as spherical wavefront and appearance and disappearance of MPCs on both time and array axis. As the dimension of the antenna array becomes large, different kinds of non-stationary properties appear across the array and different array elements may observe different receiving paths [9, 10]. Likewise, the channel components such as Rx and IOs may have relative motion, the Doppler effect should be considered in the calculations. Furthermore, a comprehensive model should consider channel characteristics in the 3D space. Due to the complexity of many propagation environments, the simplicity and applicability of the

*Corresponding Author Institutional Email: tamaddondar@itrc.ac.ir
(M. M. Tamaddondar)

Please cite this article as: M. M. Tamaddondar, N. Noori, Hybrid Massive MIMO Channel Model Based on Edge Detection of Interacting Objects and Cluster Concept, ***International Journal of Engineering, Transactions B: Applications***, Vol. 35, No. 2, (2021) 471-480

channel model are very important. In recent years, the development of a comprehensive model that can take into account various aspects of the massive MIMO channel has attracted much interest from the researchers.

1. 1. Related Massive MIMO Channel Model Many efforts have been prepared for MIMO channel modeling. Some examples of these models include European Cooperation in Science and Technology [11]. Wireless World Initiative New Radio (WINNER) + [12]. WINNER II [13]. 3D Spatial Channel Model (SCM) [14].and IMT-A models. However, such models cannot be extended to the massive MIMO systems, because most of these models consider plane wave condition in their calculations. Also, the birth-death property of the clusters cannot be observed on the array axis of MIMO system, while this phenomenon may exist in the many massive MIMO systems. Recently, several channel models have been presented for massive MIMO systems, each of which incorporates some of the features of the corresponding channel.

Several channel models for massive MIMO technology are 3D twin cluster model [15]. 3D 5G channel model [16]. 3D ellipsoid model [17]. and 2D KBSM-BD-AA [18]. have been compared and evaluated by Bai et al. [19] The visibility region method with the birth-death process is utilized to model the non-stationary property of clusters in the massive MIMO channel [20]. This model assumes spherical wavefront to capture the characteristics of AoA shifts and Doppler frequency variations because of the near-field effects. We have also presented a channel model based on the cluster concept discussed by Tamaddondar and Noori [21].

Some other channel models are presented based on the channel measurements. Measurement results at 2.6 GHz by Gao et al. [22]show that some antennas in massive MIMO systems contribute more than the others, while in i.i.d. Rayleigh channels, all antennas have equal contributions. Hence, the CIR of the channel may vary significantly over the antenna array in massive MIMO systems. Some other measurement-based channel model with their overall output results are listed in Table 1.

1. 2. Our Contributions To the best of the authors' knowledge, a comprehensive and standardized channel model for massive MIMO systems is still missing in the literatures. This paper aims to cover the specifications of the massive MIMO channels and derives a hybrid channel model. This hybrid model includes two deterministic and stochastic modes. The deterministic mode uses numerical techniques for solving Maxwell's equations by taking into account the geometry of the environment. Due to the complexity of the channel, those parts of the channel that cannot be model in the deterministic mode are considered in the stochastic mode. The edge detection technique is utilized to find scattering of MPCs. The major contributions and novelties of this paper can be summarized as follows:

1) A novel 3D hybrid channel model for massive MIMO systems is presented in this paper based on the edge detection of the IOs and cluster concepts. The central limit theorem (CLT) is utilized to simulate arrived signal to the receiver.

2) The near-field effect caused by the massive number of the antennas is considered in the proposed channel model.

3) The Doppler effect is considered in this channel model due to the relative motion of different channel components such as transmitter, receiver and IOs.

4) Appearance and disappearance of the clusters due to the huge number of antenna in the massive MIMO systems are evaluated to observe the non-stationary property of the channel on the array axis

TABLE 1. Some measurement based channel model specification for massive MIMO systems

Freq. [GHz]	Ant. Top.	Type	Scenario	Result	Ref.
13–17	40×40	Planar	Outdoor	K-factor, DS, AoA, AoD, Spatial-non-stationary	[23]
5.95–6.05	256	Rectangular	Subway	Angle distribution, angle spread, inter and intera cluster parameter	[24]
3.33	64	Linear	Outdoor	Delay and spatial non-stationary, PDP, DS, angel spread	[25]
11	4×64	Rectangular	Indoor	Power, delay, AoD, spatial-non-stationary	[26]
2,4,6	64	Linear	Indoor	Pathloss, RMS delay, coherent bandwidth, spatial non-stationary	[27]
3.5	256	Planer	Indoor/Outdoor	Capacity, eigenvalue, evolotion of cluster	[28]
11,16, 28,38	51×51,76×76, 91×91,121×121	Planer	Indoor	Spatial non-stationary, PDP, PAP, RMS DS	[29]

The rest of the paper is organized as follows. Section II gives a general description of the proposed 3D hybrid channel model for massive MIMO systems. Theoretical mathematic relations are given in section III. Some simulation results are depicted in section IV. Conclusions are finally drawn in section V.

2. PROCESS OF CHANNEL MODELING

Different aspects of the channel can be extracted in the channel modeling. Here, we try to propose a novel channel model for a standard massive MIMO system with M antenna element at the base station (BS) which serves N mobile station (MS). The propagation channel usually produces MPCs that arrive with different time delays to the users. By finding these MPCs, the CIR of the channel can be calculated. However, theoretical methods may face a huge amount of computations due to the complexity of the channel. To overcome this challenge, a novel hybrid method including both deterministic and stochastic modes is utilized to model the channel. In the deterministic mode, the line of sight (LoS) and reflection components are calculated. The equivalent planes are defined and used instead of smooth surfaces of the environment such as walls, ramps, and the ground. Then, the image theory is applied to these planes to find if any reflection path exists. The LoS or reflection paths may cross other surfaces. In such cases, the transmission coefficients are also considered in the calculations. Figure 1 shows the propagation mechanism in the deterministic mode.

The mechanism of buildings simulation is shown in Figure 2. For buildings modeling, 3D coordinates of the building's front plane quadrangle are defined clockwise. Then, by extruding the front surface along the vector of extrusion, three other surfaces of the building are completed. Finally, the ceiling and floor of the building

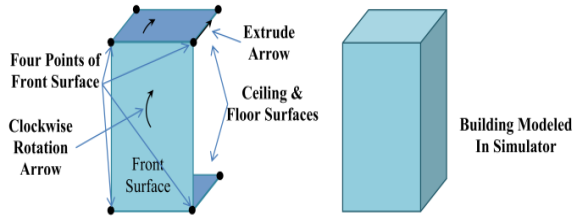

Figure 2. Procedure of building modeling in the simulator.

are defined. If the ground effect is considered, then definition of the floor is neglected.

Some parts of the channel that are too complex to be modeled in the deterministic mode are considered in the stochastic mode. Different kinds of propagation phenomena such as reflection, diffraction, and scattering occur at the edge of the IOs. These IOs are modeled with their equivalent structural geometry in the simulator as shown in Figure 3. Here, edge detection technique is utilized to distinguish the border of the IOs. Then, new MPCs are assigned to the edge of the IOs. We assume that the rays arriving at the MS follow the clustering behavior. Thus, the environment around the MS is divided into range cells (RCs). The edges of the IOs with the corresponding RCs are considered as active RCs. The MPCs may reach the MS from these active RCs. The mechanism of MPCs generation in the stochastic mode with the edge detection algorithm is shown in Figure 4. The number of MPCs in such RCs is modeled with Poisson random distribution.

The MPCs may cross the other RCs which are filled with other part of IOs. The pathloss of these IOs are considered in the calculations. Different components of the channel such as BS, MS, and IOs may have relative velocity. This causes frequency shifts due to the Doppler effect. This effect is considered in both deterministic and stochastic modes.

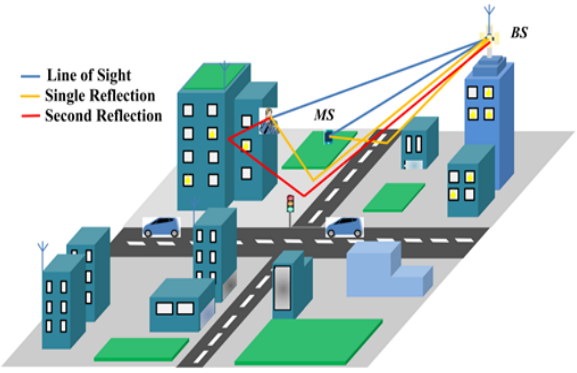

Figure 1. Model of the channel in the deterministic mode with equivalent planes

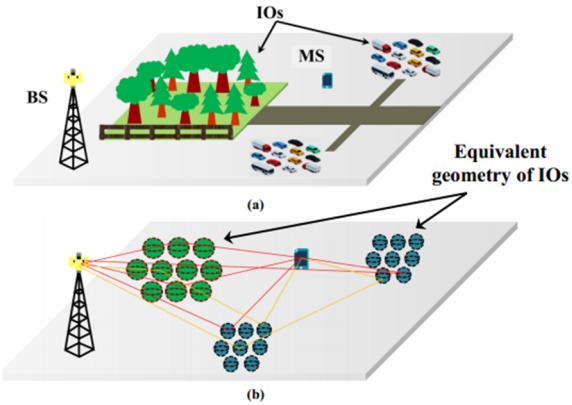

Figure 3. Illustration of a) Propagation Environment in the stochastic mode, b) Equivalent model in the simulator

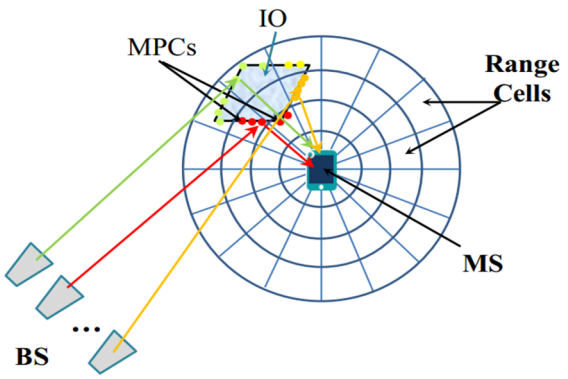

Figure 4. Mechanism of MPCs generation with edge detection algorithm

Finally, both derived deterministic and stochastic CIRs are integrated. Then the channel characteristics such as total CIR, delay spread, AoA, and ToA are extracted.

The flowchart in Figure 5 shows the presented channel modeling algorithm. As can be seen in Figure 5, several blocks are considered for channel modeling. In general, the initial parameters such as operating frequency, antenna radiation pattern, location of the BS and MS antennas, and the number of the antenna array elements with their configurations, as well as velocity vector should be defined at the first step. In the deterministic part, the equivalent surfaces are defined and in the stochastic part, the edges of the objects are drawn and the propagation environment is clustered.

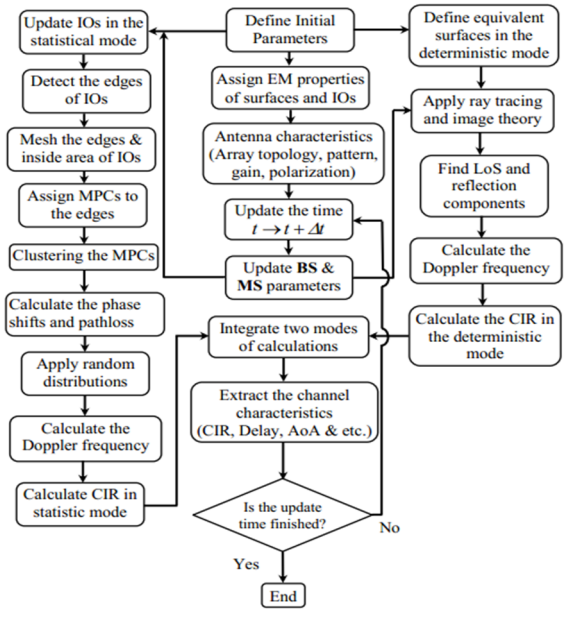

Figure 5. The flowchart of the channel modeling for massive MIMO systems

At any time instance, all time-variant variables are updated. All MPCs are found by applying ray tracing in the deterministic mode and the idea of detecting the edges of IOs in the stochastic mode. Then both deterministic and stochastic calculations are integrated. If the update time is finished, the required results will be extracted from the simulations.

Generally, deterministic channel models require geometrical information of the propagation environment, while, stochastic channel models are based on the channel statistics. In this paper, a hybrid channel model is proposed which includes two deterministic and stochastic modes. Such a channel model can be applied to a wide range of practical propagation channels. If the process of channel modeling is completely implemented in both deterministic and stochastic modes, the computational algorithm is shown in Figure 5 will extract different characteristics of a real channel. However, the deterministic mode needs geometrical information of the channel like other deterministic models.

3. MATHEMATICAL DESCRIPTION OF THE CHANNEL MODEL

The mathematical description of the channel is required for theoretical channel modeling. When an impulse is sent from a BS antenna element to the propagation environment, different MPCs may be produced and received at the MS. These MPCs pass through different propagation paths with different delay times. Regarding Figure 6, the time-variant CIR between the *m*th antenna at the BS and the *n*th user is dependent on time and delay axes.

Since the channel modeling mechanism is divided into two separate modes, the CIR can be expressed in terms of two separate channel response of deterministic and stochastic modes as follows:

$$h_{m,n}(t,\tau) = h^{d}_{m,n}(t,\tau) + h^{s}_{m,n}(t,\tau) \quad (1)$$

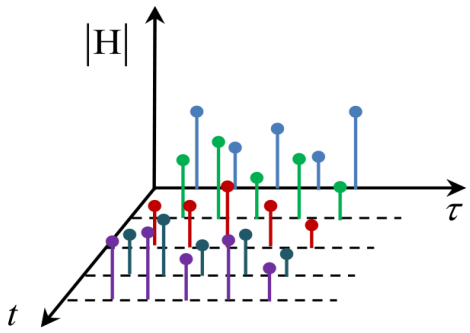

Figure 6. Time-variant channel impulse response diagram

where $h^d_{m,n}$ and $h^s_{m,n}$ are the multipath CIRs of the deterministic and stochastic modes, respectively. Here, the LoS and reflection components are calculated in the deterministic mode. Reflections up to second-order are considered in calculations. Thus the impulse response in the deterministic mode, $h^d_{m,n}$ can be rewritten as a combination of LoS and other reflection components:

$$h^d_{m,n}(t,\tau) = \sum_{i=1}^{T}\sum_{l=1}^{N_i} \alpha^d_{i,l} \exp(-j\beta r^d_{i,l}) \times \delta(\tau-\tau_l)\delta(t-t_i) \quad (2)$$

where $i = \{1,2,...,T\}$ is the total number of time instances, $\tau = \{\tau_{i,1}, \tau_{i,2}, ..., \tau_{i,N_i}\}$ is the delay series of the ith time instance. The number of MPCs in ith time instance is N_i. The propagation constant is β and the length of the lth MPC in ith time instance in the deterministic mode is denoted by $r^d_{i,l}$. The operator $\delta(\cdot)$ is the delta Dirac function. The amplitude of the MPCs in the deterministic mode is equal to:

$$\alpha^d_{i,l} = \frac{\lambda \Gamma^d_{i,l}}{4\pi r^d_{i,l}} \quad (3)$$

where $\Gamma^d_{i,l}$ is the attenuation factor related to the LoS or the first or second order reflection components and is defined by:

$$\Gamma^d_{i,l} = \begin{cases} 1 & \rightarrow \text{Line of sight} \\ \Gamma^{(1)}_{i,l} & \rightarrow \text{Reflection of the first order} \\ \Gamma^{(1)}_{i,l} \cdot \Gamma^{(2)}_{i,l} & \rightarrow \text{Reflection of the second order} \end{cases}$$

The attenuation factors of ith time instance and lth MPC for the first and second order reflections are denoted by $\Gamma^{(1)}_{i,l}$ and $\Gamma^{(2)}_{i,l}$, respectively.

As mentioned before, due to the complexity of many objects, they cannot be modeled in the deterministic mode. The stochastic mode is utilized here to overcome this problem. Here, we use this fact that different propagation phenomena such as reflection, diffraction and scattering typically occur at the boundaries of the medium discontinuities. Thus, an edge detection algorithm is proposed to diagnose the boundaries of the IOs. Accordingly, the boundaries and inner areas of the IOs are meshed separately for detecting boundaries and inner area of the IOs. The MPCs are attributed to the outer boundaries of the IOs. Simultaneously, as the propagation of MPCs has clustering behavior, the clustering technique is applied in the MS side to categorize the MPCs. Some characteristics of these MPCs are extracted by using random distributions. With such explanations, the CIR in the stochastic mode can be defined in the following form:

$$h^s_{m,n}(t,\tau) = \sum_{i=1}^{T}\sum_{c=1}^{C}\sum_{l=1}^{L^s_c} \alpha^s_{l,c,i} \exp(-j\phi_{l,c,i}) \times \delta(\tau-\tau_l)\delta(t-t_i) \quad (4)$$

where $c = \{1,2,...,C\}$ is the number of clusters, $\alpha^s_{l,c,i}$ and $\phi_{l,c,i}$ are the amplitude and phase shift of lth MPCs in the stochastic mode at the ith time instance in the cth cluster, respectively. The amplitude can be given by:

$$\alpha^s_{l,c.i} = \frac{\lambda D^s_{l,c,i}}{4\pi r^s_{l,c.i}} \quad (5)$$

The diffraction or scattering coefficient in the stochastic mode is denoted by $D^s_{l,c,i}$ and $r^s_{l,c,i}$ is the path length of the lth MPC at the ith time instance in the cth cluster. The phase shift of each MPC is obtained from a uniform distribution between $[0, 2\pi)$. Also, Poisson distribution is used to compute the number of MPCs of the cth cluster, L^s_c. Regarding the density of the propagation environment (sparse, medium or dense environments), and based on the various simulations such as what has been presented in [21], the proper average number of MPCs has been obtained between zero and five. In other words, as the diffraction parts of an IO are increased, the average number of MPCs used in Poisson distribution is also increased and vice versa.

The MPCs that arrive to the MS in each delay bin are summed with each other. It means that:

$$h_{m,n}(t,\tau_k) = \sum_{p=1}^{P_k} h_{m,n}(t,\tau_p)$$
$$\tau_k - \frac{\Delta\tau}{2} < \tau_p < \tau_k + \frac{\Delta\tau}{2} \quad (6)$$
$$\tau_k = k\Delta\tau, \qquad k = 0,1,2,...,K$$

where K is total number of successive delay bins and $p = \{1,2,...,P_k\}$ is the number of MPCs in the kth delay bin. The width of each delay bin is $\Delta\tau$. Both slow and fast fading are obtained during the channel simulations since the amplitude and phase of all received MPCs are calculated.

The average power delay profile (APDP) is generally used to calculate delay spread and remove impacts of the noise in time-invariant channel. It can be obtained from the PDP samples of the ith time instance which is defined as follows:

$$APDP_{m,n}(\tau_K) = \frac{1}{N_{cyc}} \sum_{i=1}^{N_{cyc}} PDP_{m,n}(\tau, t_i) \quad (7)$$

$$PDP_{m,n}(\tau,t_i)=\left|h_{m,n}(\tau,t_i)\right|^2 \tag{8}$$

where N_{cyc} is the number of PDP samples between the mth antenna of the BS and the nth user and t_i is the ith time instance. It should be emphasized that Equation (7) is considered for such a channel that is stationary on time axis. For time-variant channels, the samples should be taken in the duration of coherence time. Then, the root mean square (RMS) delay spread can be calculated using APDP as follows:

$$\tau_{rms}=\sqrt{\frac{\sum_q APDP(\tau_q)\tau_q^2}{\sum_q APDP(\tau_q)}-\left(\frac{\sum_q APDP(\tau_q)\tau_q}{\sum_q APDP(\tau_q)}\right)^2} \tag{9}$$

The AoA is another useful parameter which shows the angle of MPCs arrived to the MS. This parameter is used in the clustering of MPCs. The AoAs in elevation and azimuth planes are shown by θ_{AoA} and φ_{AoA}, respectively and defined as:

$$\theta_{AoA}=\cos^{-1}\left(\frac{\mathbf{a_z}\cdot\mathbf{IR}}{|\mathbf{IR}|}\right) \tag{10}$$

$$\varphi_{AoA}=\cos^{-1}\left(\frac{\mathbf{a_x}\cdot\mathbf{IR}}{|\mathbf{IR}|}\right) \tag{11}$$

where, the vector point from the IO to the MS is **IR** and $\mathbf{a_x}$ and $\mathbf{a_z}$ are the unit vectors on the x and z axes, respectively. Both AoA and time delay are used to separate arrival rays of different clusters. In fact, rays with similar AoAs and delays make one cluster. The MPCs are categorized by considering their time delay and AoAs using the K-mean algorithm. The paths of some MPCs go through clusters which are filled with IOs. Thus, the phase shifts and the pathloss due to these clusters are also added to total calculations.

3. 1. Antenna The channel response depends on the antenna characteristics such as radiation pattern and gain. Since in massive MIMO systems, the radiation pattern can be affected by adjacent antenna elements, the radiation pattern of the antenna element in the array are imported into the calculations. As the near-field effect may influence on the response of the channel, the radiation pattern of the antenna is calculated in the required distance from the antenna element. Therefore, the CIR in both deterministic and stochastic modes can be rewritten as follows:

$$\begin{aligned}h^d_{m,n}(t,\tau)=&\sum_{i=1}^{T}\sum_{l=1}^{N_i}\alpha^d_{l,i}\exp(-j\beta r^d_{l,i})\times\\ &F^{Tx}_m(R^{Tx}_{l,i},\theta^{Tx}_{l,i},\varphi^{Tx}_{l,i})\cdot F^{Rx}_n(R^{Rx}_{l,i},\theta^{Rx}_{l,i},\varphi^{Rx}_{l,i})\times\\ &\delta(\tau-\tau_l)\cdot\delta(t-t_i)\end{aligned} \tag{12}$$

$$\begin{aligned}h^s_{m,n}(t,\tau)=&\sum_{i=1}^{T}\sum_{c=1}^{C}\sum_{l=1}^{L^s_c}\alpha^s_{l,c,i}\exp(-j\phi^s_{l,c,i})\times\\ &F^{Tx}_m(R^{Tx}_{l,c,i},\theta^{Tx}_{l,c,i},\varphi^{Tx}_{l,c,i})\cdot F^{Rx}_n(R^{Rx}_{l,c,i},\theta^{Rx}_{l,c,i},\varphi^{Rx}_{l,c,i})\times\\ &\delta(\tau-\tau_{l,c})\cdot\delta(t-t_i)\end{aligned} \tag{13}$$

where F^{Tx}_m and F^{Rx}_n are the radiation pattern of the mth antenna element at the BS and the nth MS, respectively. The observation distances from BS and MS in spherical coordinates are $(R^{Tx}_{l,c,i},\theta^{Tx}_{l,c,i},\varphi^{Tx}_{l,c,i})$ and $(R^{Tx}_{l,c,i},\theta^{Tx}_{l,c,i},\varphi^{Tx}_{l,c,i})$, respectively.

3. 1. Doppler Effect Since the channel components typically have relative velocity, there is a Doppler effect in the channel. Accordingly, the Doppler frequency is calculated and considered in the CIR. Regarding Figure 7, the Doppler frequency can be expressed as follows:

$$f_D=f_{obs1}\left(1+\frac{v_{IO}\cos\theta_{IO,Rx}}{c_0}\right)\left(1+\frac{v_{Rx}\cos\theta_{Rx,IO}}{c_0}\right) \tag{14}$$

$$f_{obs1}=f_c\left(1+\frac{v_{Tx}\cos\theta_{Tx,IO}}{c_0}\right)\left(1+\frac{v_{IO}\cos\theta_{IO,Tx}}{c_0}\right) \tag{15}$$

where f_c is the carrier frequency and c_0 is the velocity of the transmitted signal. The v_{Tx}, v_{IO} and v_{Rx} are the velocity vectors of the Tx, IO and Rx, respectively. The angles $\theta_{Tx,IO}$, $\theta_{IO,Tx}$, $\theta_{IO,Rx}$ and $\theta_{Rx,IO}$ are shown in Figure 7.

The locations of the BS and MS with their corresponding velocity vectors as well as the location and velocity vector of IOs are imported into the simulator. The simulator computes the required angles

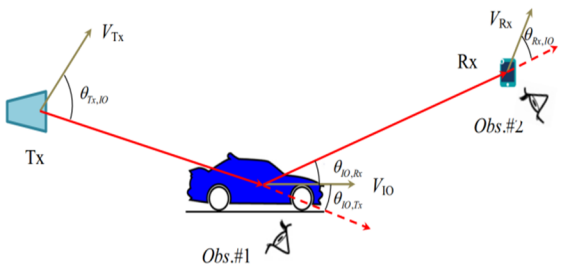

Figure 7. Illustration of parameters for Doppler effect calculations

for the Doppler frequency calculation based on the departure and arrival angles of each observation point. This information is used to implement in Equations (14) and (15) to model and calculate Doppler effect of each path.

4. SIMULATION AND RESULTS

In this section, simulations are carried out to extract channel characteristics. An outdoor propagation environment is defined to implement the proposed channel model. This channel includes several buildings, ground effect, car parking and garages. These obstacles are defined in our simulations based on the procedure of deterministic and stochastic modes presented in previous sections. Accordingly, the buildings and ground are modeled with their equivalent surfaces. However, the other parts of the channel including garages and car parking are modeled by stochastic mode as IOs with their edge boundaries (as depicted in Figure 3). The geometrical schematic of this channel is shown in Figure 8. The buildings and the ground as well as three IOs are depicted in this figure. The ray tracing algorithm is utilized to find all paths between the BS and MS which is shown in Figure 8. The LoS, as well as the first and second order reflection components is calculated in the deterministic mode. The edge detection algorithm is used to distinguish the MPCs in the stochastic mode.

At first, the received power at the MS is obtained versus the distances between transmitter and receiver where BS and MS antennas have omni-directional radiation pattern. The obtained results of the proposed channel model are compared with those obtained by classic ray tracing method. This comparison is shown in Figure 9. In the ray tracing model, only the LoS and reflections are considered in the calculations, while in the proposed model, in addition to the deterministic mode components, the cluster behavior of the channel is also included in the calculations. Thus, the proposed model considers more details of the channel in comparison with the ray tracing model.

Then, the simulations are done for a massive MIMO system including a 256-element antenna at the BS. The number of 256 elements represents a massive MIMO system, in which we want to show the non-stationary property of the channel along the array. The antenna element is placed in a linear configuration with half of the wavelength distance between successive elements. The frequency of simulation is set to 28 GHz since this frequency is a candidate for realizing millimeter-wave massive MIMO systems. All parameters of the considered system are listed in Table 2.

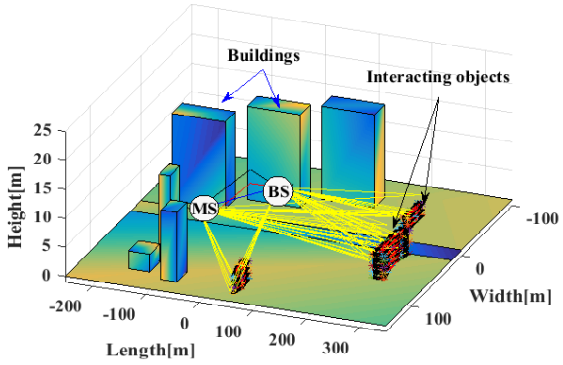

Figure 8. The propagation environment in the simulator

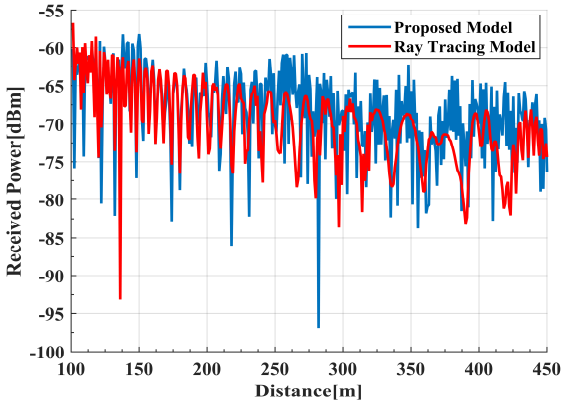

Figure 9. Received power versus the distance between the first antenna at BS and MS

TABLE 2. Preliminary Definitions in the simulations

Carrier Frequency : 28 GHz
BS Antenna: 256–Open-Ended Element, Linear Array, Vertical Polarization, Directive Pattern
MS Antenna: Single Dipole, Vertical Polarization, Omnidirectional Pattern
Transmit Power : 1W
BS Center Position: [120, 120, 18]
MS Position : [13, -130, 1.5]
MS Velocity Vector : $[\frac{17\sqrt{2}}{2}, \frac{17\sqrt{2}}{2}, 0]$
Building Characteristics : $\varepsilon_r = 4.1\ \mu_r = 1\ \sigma = 0.001$
IO Characteristics : $\varepsilon_r = 1\ \mu_r = 1\ \sigma = 1.45e6$

*The coordinates of the points are in meter.

The PDP with respect to the delay of the MPCs are depicted in Figure 10. This PDP can be considered as the CIR of the first antenna element at the BS and the MS. Different kinds of MPCs are separated in the simulation as shown in Figure 10. These MPCs include LoS, reflections of the first-order from one wall, reflection of the second-order from two walls, and single bounce components due to diffraction or scattering from IOs. Hence, these different MPCs are originated from different paths and propagation phenomena. The LoS component has the highest strength among all MPCs, while the MPCs from IOs have lower strengths in overall look of Figure 10. The threshold level is considered to be -160 dBm in the simulations. The AoAs in both elevation and azimuth planes are derived in the simulations. Thus, the PAP between the first BS antenna element and the MS with respect to the AoAs is shown in Figure 11. The cluster behavior of the MPCs can be viewed in both Figures 10 and 11. Since the distance between the array elements at the BS is low at 28 GHz, the sub-arrays in the massive MIMO system almost experience a stationary channel. However, the non-stationary property between these sub-arrays is significant.

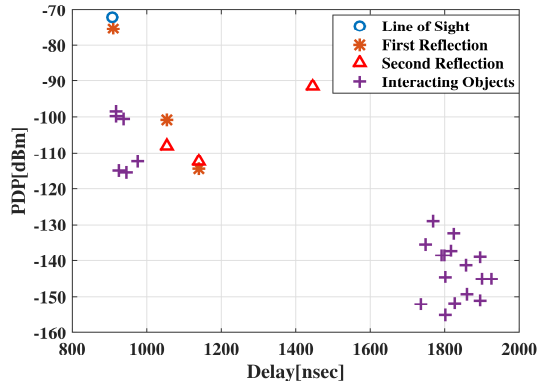

Figure 10. Power delay profile between the first Antenna at BS and MS with respect to the delay of MPCs

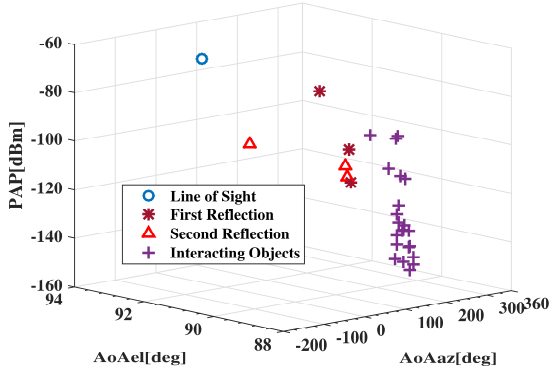

Figure 11. Power angle profile with respect to the angle of arrival

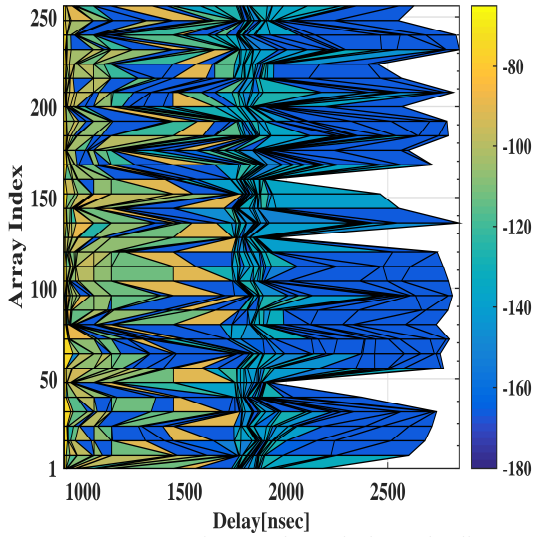

Figure 12. Non-Stationary channel along the linear array antenna with 256 elements

Figure 12 shows the non-stationary property of the channel along the array axis for 256-element antenna at the BS. The main reason of this phenomenon is that due to the huge number of the antenna elements and large size of the array against operating frequency wavelength, different channels are experienced along the massive MIMO array by distinct elements.

Here, the Doppler effect is considered in the simulations. As mentioned in Table 2, the MS has a relative velocity which causes a Doppler shift. The Doppler shift of the frequency for each MPC is shown in Figure 13. This shows that the Doppler shift of the frequency is about 3 kHz in this scenario.

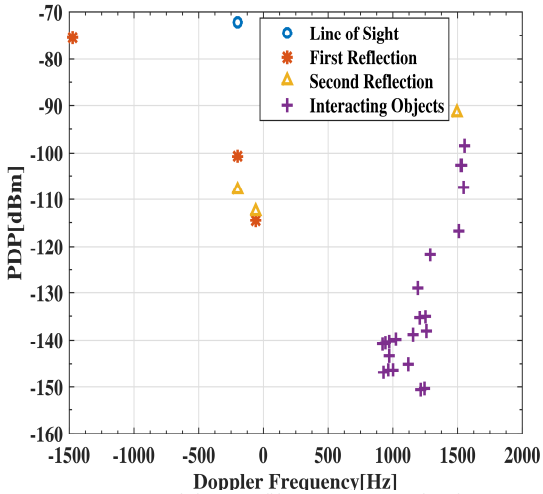

Figure 13. Power delay profile versus Doppler frequency

5. SUMMARY AND CONCLUSION

In this paper, we have proposed a novel channel model for massive MIMO systems. This hybrid channel model includes deterministic and stochastic modes. The smooth surfaces are defined in the deterministic mode. Then the ray tracing algorithm is utilized to find the LoS component along with the first and second order reflections. Other parts of the channel are defined in the stochastic mode. In this mode, the edge detection algorithm is used to find the boundaries of the IOs. This is because of the fact that different propagation phenomenon such as reflection, diffraction and scattering often occurred at the boundaries of the objects. Thus the MPCs are assigned to the outer edges of the IOs. The relative motion of the channel components cause Doppler shifts in the frequency. This Doppler effect is considered in this channel model to have a better overview of the received signals at the MS. Finally, the MPCs from both deterministic and stochastic modes are integrated to extract the desired characteristics of the channel such as CIR, delay spread, AoAs and Doppler shifts. The non-stationary property of the massive MIMO channel is observed in the simulation. This channel model can be considered as a time-variant channel model due to the capability of updating all channel specifications such as antenna positions and velocity vectors of the BS and MS in each snapshot.

6. REFERENCES

1. Jiang, H., Tang, D., Zhou, J., Xi, X., Feng, J., Dang, J. and Wu, L.J.I.A., "Approximation algorithm based channel estimation for massive mimo antenna array systems", ***IEEE Access*** Vol. 7, (2019), 149364-149372, doi: 10.1109/ACCESS.2019.2947533
2. El Misilmani, H. and El-Hajj, A., "Massive mimo design for 5g networks: An overview on alternative antenna configurations and channel model challenges", in 2017 International Conference on High Performance Computing & Simulation (HPCS), IEEE. (2017), 288-294.
3. Larsson, E.G., Edfors, O., Tufvesson, F. and Marzetta, T.L.J.I.c.m., "Massive mimo for next generation wireless systems", ***IEEE Communications Magazine*** Vol. 52, No. 2, (2014), 186-195, doi: 10.1109/MCOM.2014.6736761
4. Lu, L., Li, G.Y., Swindlehurst, A.L., Ashikhmin, A. and Zhang, R.J.I.j.o.s.t.i.s.p., "An overview of massive mimo: Benefits and challenges", ***IEEE Journal of Selected Topics in Signal Processing*** Vol. 8, No. 5, (2014), 742-758, doi: 10.1109/JSTSP.2014.2317671
5. Gao, X., Edfors, O., Rusek, F. and Tufvesson, F.J.I.T.o.W.C., "Massive mimo performance evaluation based on measured propagation data", ***IEEE Transactions on Wireless Communications*** Vol. 14, No. 7, (2015), 3899-3911, doi: 10.1109/TWC.2015.2414413
6. Nielsen, J.O., Fan, W., Eggers, P.C. and Pedersen, G.F.J.I.C.M., "A channel sounder for massive mimo and mmwave channels", ***IEEE Communications Magazine*** Vol. 56, No. 12, (2018), 67-73, doi: 10.1109/MCOM.2018.1800199
7. Sayeed, A.M.J.I.T.o.S.p., "Deconstructing multiantenna fading channels", IEEE Transactions on Signal processing Vol. 50, No. 10, (2002), 2563-2579, doi: 10.1109/TSP.2002.803324
8. Bazzi, S., Stefanatos, S., Le Magoarou, L., Hajri, S.E., Assaad, M., Paquelet, S., Wunder, G. and Xu, W.J.I.A., "Exploiting the massive mimo channel structural properties for minimization of channel estimation error and training overhead", ***IEEE Access*** Vol. 7, (2019), 32434-32452, doi: 10.1109/ACCESS.2019.2903654
9. Ali, A., De Carvalho, E. and Heath, R.W.J.I.W.C.L., "Linear receivers in non-stationary massive mimo channels with visibility regions", IEEE Wireless Communications Letters Vol. 8, No. 3, (2019), 885-888, doi: 10.1109/LWC.2019.2898572
10. Martínez, À.O., De Carvalho, E. and Nielsen, J.Ø., "Towards very large aperture massive mimo: A measurement based study", in 2014 IEEE Globecom Workshops (GC Wkshps), IEEE., (2014), 281-286.
11. Liu, L., Oestges, C., Poutanen, J., Haneda, K., Vainikainen, P., Quitin, F., Tufvesson, F. and De Doncker, P.J.I.W.C., "The cost 2100 mimo channel model", ***IEEE Wireless Communications*** Vol. 19, No. 6, (2012), 92-99, doi: 10.1109/MWC.2012.6393523
12. Meinila, J., Kyosti, P. and Hentila, L., "Winner+ final channel models", Wireless World Initiative New Radio WINNER, (2010), doi:
13. Döttling, M., Mohr, W. and Osseiran, A., "Radio technologies and concepts for imt-advanced, John Wiley & Sons, John Wiley \& Sons (2009).
14. Tennakoon, P. and Wavegedara, C.B., "A 3d geometry-based spatial correlation model for mimo channels", in 2019 Moratuwa Engineering Research Conference (MERCon), IEEE. (2019), 222-227.
15. Wu, S., Wang, C.-X., Alwakeel, M.M. and He, Y.J.I.j.o.s.a.i.c., "A non-stationary 3-d wideband twin-cluster model for 5g massive mimo channels", ***IEEE Journal on Selected Areas in Communications,*** Vol. 32, No. 6, (2014), 1207-1218, doi: 10.1109/JSAC.2014.2328131
16. Wu, S., Wang, C.-X., Alwakeel, M.M. and You, X.J.I.T.o.C., "A general 3-d non-stationary 5g wireless channel model", ***IEEE Transactions on Communications,*** Vol. 66, No. 7, (2017), 3065-3078, doi: 10.1109/TCOMM.2017.2779128
17. Bai, L., Wang, C.-X., Wu, S., Wang, H. and Yang, Y., "A 3-d wideband multi-confocal ellipsoid model for wireless mimo communication channels", in 2016 IEEE International Conference on Communications (ICC), IEEE. (2016), 1-6.
18. Wu, S., Wang, C.-X., Aggoune, E.-H.M. and Alwakeel, M.M., "A novel kronecker-based stochastic model for massive mimo channels", in 2015 IEEE/CIC International Conference on Communications in China (ICCC), IEEE., (2015), 1-6.
19. Bai, L., Wang, C.-X., Wu, S., Lopez, C.F., Gao, X., Zhang, W. and Liu, Y., "Performance comparison of six massive mimo channel models", in 2017 IEEE/CIC International Conference on Communications in China (ICCC), IEEE. (2017), 1-5.
20. Chen, J.-q., Zhang, Z., Tang, T., Huang, Y.-z.J.F.o.I.T. and Engineering, E., "Anon-stationary channelmodel for 5gmassive mimosystems", ***Frontiers of Information Technology \& Electronic Engineering*** Vol. 18, No. 12, (2018), 2101-2110, doi: 10.1631/FITEE.1700028
21. Tamaddondar, M.M. and Noori, N., "3d massive mimo channel modeling with cluster based ray tracing method", in 2019 27th Iranian Conference on Electrical Engineering (ICEE), IEEE. (2019), 1249-1253.
22. Gao, X., Edfors, O., Tufvesson, F. and Larsson, E.G.J.I.T.o.C., "Massive mimo in real propagation environments: Do all antennas contribute equally?", ***IEEE Transactions on Communications*** Vol. 63, No. 11, (2015), 3917-3928, doi: 10.1109/TCOMM.2015.2462350

23. Chen, J., Yin, X. and Wang, S., "Measurement-based massive mimo channel modeling in 13–17 ghz for indoor hall scenarios", in 2016 IEEE International Conference on Communications (ICC), IEEE. (2016), 1-5.

24. Li, J., Ai, B., He, R., Yang, M., Wang, Q., Zhang, B. and Zhong, Z.J.I.A., "Cluster-based 3-d channel modeling for massive mimo in subway station environment", ***IEEE Access,*** Vol. 6, (2017), 6257-6272, doi: 10.1109/ACCESS.2017.2779119

25. Fei, D., He, R., Ai, B., Zhang, B., Guan, K. and Zhong, Z., "Massive mimo channel measurements and analysis at 3.33 ghz", in 2015 10th international conference on Communications and Networking in China (ChinaCom), IEEE. (2015), 194-198.

26. Li, J., Ai, B., He, R., Yang, M., Zhong, Z., Hao, Y. and Shi, G., "The 3d spatial non-stationarity and spherical wavefront in massive mimo channel measurement", in 2018 10th International Conference on Wireless Communications and Signal Processing (WCSP), IEEE. (2018), 1-6.

27. Li, J., Ai, B., He, R., Guan, K., Wang, Q., Fei, D., Zhong, Z., Zhao, Z., Miao, D. and Guan, H., "Measurement-based characterizations of indoor massive mimo channels at 2 GHZ, 4 ghz, and 6 ghz frequency bands", in 2016 IEEE 83rd Vehicular Technology Conference (VTC Spring), IEEE. (2016), 1-5.

28. Zhang, J., Wang, C., Wu, Z. And Zhang, W.J.Z.C., "A survey of massive mimo channel measurements and models", ***ZTE Communications*** Vol. 15, No. 1, (2017), doi: 10.1155/2014/848071

29. Huang, J., Feng, R., Sun, J., Wang, C.-X., Zhang, W. and Yang, Y., "Multi-frequency millimeter wave massive mimo channel measurements and analysis", in 2017 IEEE International Conference on Communications (ICC), IEEE., (2017), 1-6.

Persian Abstract

چکیده

این مقاله، مدل کانال جدیدی را برمبنای آشکارسازی لبه‌های اشیاء متعامل برای سیستم‌های چندورودی چندخروجی انبوه بی‌سیم ارائه می‌کند. ایده مدل کانال براین اساس است که پدیده‌های انتشار امواج الکترومغناطیسی نظیر بازتابش‌ها، پراش، پراکندگی و انکسار غالباً در لبه اشیاء متعامل تولید می‌شوند. این مدل کانال همچنین از مفهوم خوشه‌بندی برای مدل کردن مؤلفه‌های چندمسیری استفاده می‌کند. شرایط متغیر بازمان بودن کانال و وجود اثر داپلر در مدل‌سازی کانال در نظر گرفته می‌شود. پدیده غیر ایستایی کانال در امتداد محور آرایه آنتن ایستگاه پایه در شبیه‌سازی قابل مشاهده می‌باشد. به‌دلیل تعداد زیاد عناصر آرایه آنتن در ایستگاه پایه در سیستم‌های چندورودی چندخروجی انبوه، شرایط جبهه موج کروی به جای جبهه موج تخت در فواصل نزدیک در نظر گرفته می‌شود. به منظور مدل کردن مؤلفه‌های چندمسیری در هر خوشه از قضیه تئوری حد مرکزی استفاده شده و پس از مدل‌سازی کانال انتشار، مشخصه‌های آن نظیر پاسخ ضربه کانال، زوایای ورود و زمان ورود از شبیه‌سازی‌ها استخراج می‌شود.